

PAPER • OPEN ACCESS

High transmission from 2D periodic plasmonic finite arrays with sub-20 nm gaps realized with Ga focused ion beam milling

To cite this article: Filippo Pisano *et al* 2020 *Nanotechnology* **31** 435301

View the [article online](#) for updates and enhancements.

You may also like

- [Ratiometric fluorescence assay for L-Cysteine based on Fe-doped carbon dot nanozymes](#)

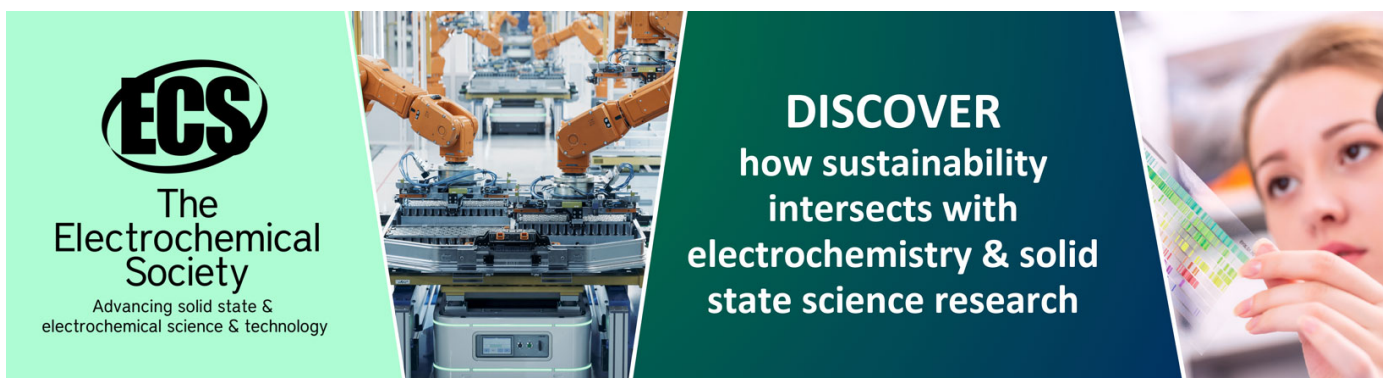
Changfang Lu, Yao Liu, Qin Wen et al.

- [Roadmap on emerging hardware and technology for machine learning](#)

Karl Berggren, Qiangfei Xia, Konstantin K Likharev et al.

- [Neon and helium focused ion beam etching of resist patterns](#)











Deying Xia, Xiaoli Zhu, Fouzia Khanom et al.



ECS
The
Electrochemical
Society
Advancing solid state &
electrochemical science & technology

DISCOVER
how sustainability
intersects with
electrochemistry & solid
state science research

High transmission from 2D periodic plasmonic finite arrays with sub-20 nm gaps realized with Ga focused ion beam milling

Filippo Pisano¹ , Antonio Balena^{1,2} , Muhammad Fayyaz Kashif³ , Marco Pisanello¹ , Gaia de Marzo^{1,2} , Luciana Algieri¹ , Antonio Qualtieri¹ , Leonardo Sileo¹, Tiziana Stomeo¹ , Antonella D'Orazio^{3,4}, Massimo De Vittorio^{1,2,4}, Ferruccio Pisanello^{1,4}  and Marco Grande^{3,4} 

¹ Fondazione Istituto Italiano di Tecnologia, Center for Biomolecular Nanotechnologies, Arnesano (LE) 73010, Italy

² Dipartimento di Ingegneria Dell'Innovazione, Università del Salento, Lecce 73100, Italy

³ Dipartimento di Ingegneria Elettrica e dell'Informazione, Politecnico di Bari, Bari, Italy

E-mail: filippo.pisano@iit.it

Received 28 May 2020, revised 30 June 2020

Accepted for publication 13 July 2020

Published 6 August 2020



Abstract

Fabricating plasmonic nanostructures with good optical performances often requires lengthy and challenging patterning processes that can hardly be transferred to unconventional substrates, such as optical fiber tips or curved surfaces. Here we investigate the use of a single Ga focused ion beam process to fabricate 2D arrays of gold nanoplatelets for nanophotonic applications. While observing that focused ion beam milling of crossing tapered grooves inherently produces gaps below 20 nm, we provide experimental and theoretical evidence for the spectral features of grooves terminating with a sharp air gap. We show that transmission near 10% can be obtained via two-dimensional nano-focusing in a finite subset of 2D arrays of gold nanoplatelets. This enables the application of our nanostructure to detect variations in the refractive index of thin films using either reflected or transmitted light when a small number of elements are engaged.

Keywords: focused ion beam, nanoplatelets, plasmonic nanostructures

(Some figures may appear in colour only in the online journal)

1. Introduction

Research in the fabrication of metallic periodic nanostructures that support surface plasmon resonances (SPR) has

received longstanding interest from both a fundamental and an applied perspective. In the past few years, the comprehensive knowledge of the resonant mechanisms in periodic arrays of sub-wavelength apertures [1–5] has been widely applied in the detection of electro-chemical signals at extremely low molecular concentrations [6–8]. This interest has been revived by the emergence of lab-on-fiber platforms, which have raised the demand for techniques to pattern unconventional substrates, such as the tip of an optical fiber, where conventional methods such as electron beam lithography cannot be applied [9]. In this endeavor, focused ion beam (FIB) milling has been identified as a versatile technique to prototype

⁴ These authors jointly supervised this work.



Original content from this work may be used under the terms of the [Creative Commons Attribution 4.0 licence](https://creativecommons.org/licenses/by/4.0/). Any further distribution of this work must maintain attribution to the author(s) and the title of the work, journal citation and DOI.

photonic structures and metasurfaces [10–12]. However, while the effect of FIB milling on 1D periodic structures has been extensively studied [13], little work—to the best of our knowledge—has been dedicated to extend this concept to 2D structures with crossing corrugations. In this work, we describe the optical properties of finite subsets in 2D arrays of gold nanoplatelets (NPs) [14] fabricated in a single Ga FIB patterning process. As FIB milling generates tapered slits, which have been shown to boost extraordinary optical transmission through adiabatic nano-focusing in 1D arrays [15], we numerically and experimentally expand this effect to comprehensively describe the optical performances of a finite subset of a 2D NPs array.

We found that FIB milling of crossing tapered grooves inherently generates sub-20 nm gaps. This is an interesting aspect since a spacing of less than 40 nm between nanostructures has been previously shown to strongly contribute to surface enhancement of Raman scattering (SERS) [16]. While observing that the orientation of such gaps with respect to the polarization of the incoming light influences the array's performance, we measured transmissivity peaks approaching 10% in the VIS–NIR region. As a possible application, we experimentally and numerically demonstrate that illuminating a subset of the array results in the detection of refractive index (RI) changes with a sensitivity of $S_R = 620 \text{ nm RIU}^{-1}$ and a figure of merit (FOM) of $\text{FOM}_R = 7 \text{ RIU}^{-1}$ using reflected light and $S_T = 445 \text{ nm RIU}^{-1}$ and a $\text{FOM}_T = 29 \text{ RIU}^{-1}$ using transmitted light. These values are consistent with previous reports for this class of devices [8].

2. Results and discussion

We fabricated NP arrays in a gold film deposited on a quartz microscope coverslip (Ted Pella), following the design shown in figures 1(a) and (b). The patterning process involved two steps. First, a 5 nm thick adhesion layer of Cr and a 180 nm thick layer of Au were deposited by electron beam deposition. Second, the NPs were carved in the gold layer by milling thin slits of metal with a Ga+ FIB system (FEI dual-beam HeliosNanoLab600i). The ion beam current was set at 7.7 pA, with 30 kV voltage. The beam spot (12 nm in diameter) was sequentially scanned in the two milling directions (from edge to edge), horizontal (H) and vertical (V) covering one gap at a time across the full array length, with minimal line overlap (5%–10%). The fabrication of a single array, $30 \mu\text{m} \times 30 \mu\text{m}$ wide, lasted for approximately 30 min. We first performed a morphological characterization of the final device via scanning electron microscope (SEM) (figure 1(b)). Interestingly, we found that the milling order influences the groove shape. This is shown in figure 1 for arrays where vertical (V) slits were milled before horizontal (H) ones. Once the set of V slits is carved, milling in the H direction produces a redeposition of sputtered material that narrows the V groove at the NP corners (figure 1(b)-inset). At the same time, the H groove widens at the platelet corners (figures 1(b)-inset, (c), and (d)). As highlighted in the SEM images, this process produces gaps approaching 10 nm in width (figure 1(b)-inset and (d)). This effect was confirmed by reversing the fabrication order of the

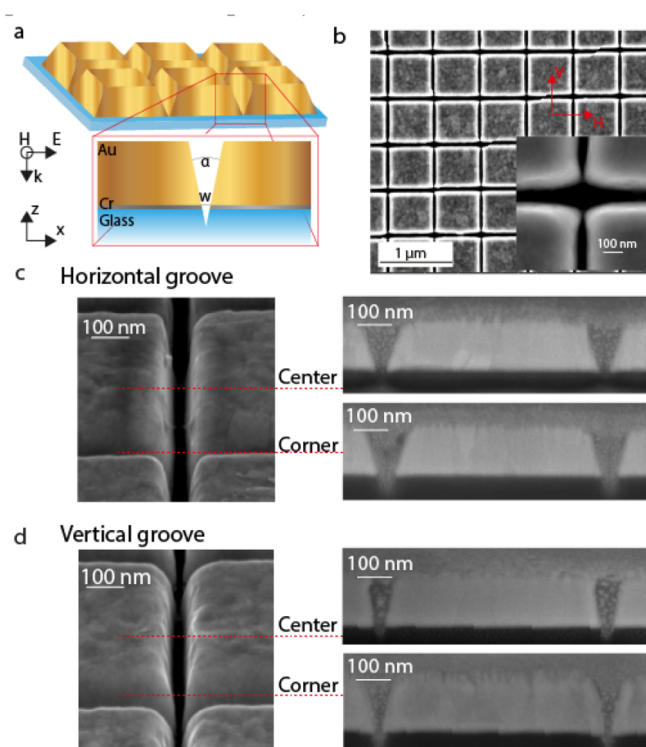


Figure 1. (a) Design of nanoplatelet array. The inset shows a close up of the tapered groove extending into the substrate. (b) In-plane SEM micrograph of a TNP array with $P = 630 \text{ nm}$. (Inset) Close-up on the nanoplatelet corner, with a gap width approaching 10 nm. (c) (Left) Tilted SEM image of a groove in the horizontal direction, showing the groove widening at the corners; (right) SEM image of the horizontal groove's cross-section at the center (top) and at the corner (bottom) of the nanoplatelet. (d) As in (c) for a groove in the vertical direction. Platinum was deposited on top of the gold layer via Ion Beam Induced Deposition to protect the nanoplatelets during the cross-section cut.

slits (figure 3(a)). We attribute this phenomenon to the combination of the edge effect and the redeposition of sputtered material.

As expected, FIB milling resulted in tapered grooves. In details, we milled grooves with a bottom aperture of $\sim 30 \text{ nm}$ at the NP center and $\sim 10 \text{ nm}$ at the corner, with an air gap extending down to $\sim 30 \text{ nm}$ below the substrate surface (figures 1(c) and (d)).

We then characterized the spectral response for two array periodicities, A and B with $P_A = 550 \text{ nm}$ and $P_B = 630 \text{ nm}$. For each periodicity, we produced arrays with reversed milling order A1 (B1), starting from the V direction, and A2 (B2) starting from the H direction. As shown in figures 3(a) and (d), the milling order influences the orientation of the narrow gaps at the NP corners. We acquired reflectance and transmittance spectra using a modified upright microscope. The experimental setup is shown in figure 2. We used a broadband light source (500–900 nm) that was spatially filtered with a $100 \mu\text{m}$ pinhole. After passing through a linear polarizer, the illumination beam was relayed on the sample, at normal incidence, using a lens (focal length 250 mm), two beam splitters (non-polarizing, 50/50) and an infinity corrected objective ($5\times$, $\text{NA} = 0.16$). We then collected reflected

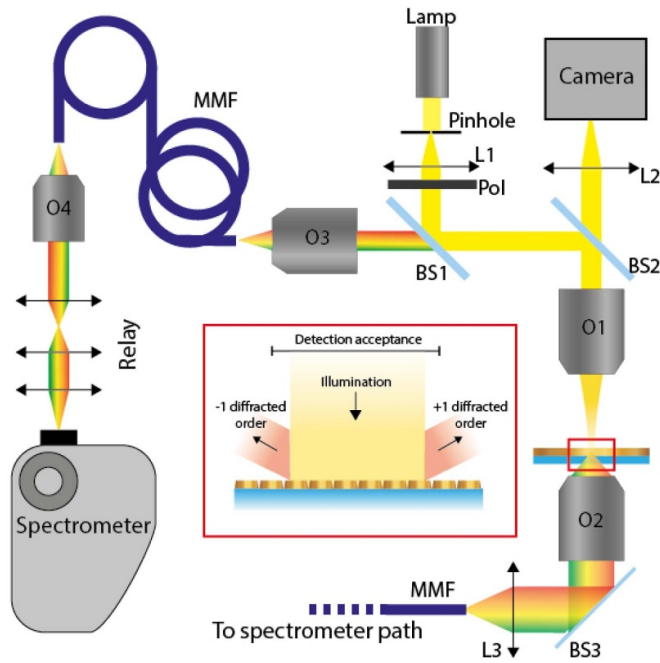


Figure 2. Sketch of the experimental system. White light is filtered with a 100 μm pinhole and linear polarizer (Pol). The image of the pinhole is projected on a subset of the NP array using a lens (L1, focal 250 mm) and an infinity corrected objective (O1, 5 \times , NA = 0.16). An imaging path is used to align the focal spot with the sample. Reflected light is collected by O1 and focused in a NA = 0.39 multimode fiber (MMF) by objective O3 (20 \times , NA = 0.5). The MMF conveys the signal to a high NA objective O4 (40 \times , NA = 0.65) that projects it to a spectrometer equipped with a 300 l mm^{-1} grating (Horiba Scientific iHR320, EMCCD camera Horiba Scientific Synapse, 1600 \times 1200 pixels). The transmitted light is collected with an infinity corrected objective (O2, 20 \times , NA = 0.5) and focused in an MMF with an achromatic doublet lens (L3, focal 40 mm). The MMF conveys the signal to the spectrometer. The inset shows an enlarged view of the excitation beam recruiting a finite number of NPs.

light with the same objective and the transmitted signal with a 20 \times objective (NA = 0.50). Spectra were recorded with a spectrometer equipped with a 300 l mm^{-1} grating (Horiba Scientific iHR320, EMCCD camera Horiba Scientific Synapse, 1600 \times 1200 pixels).

Reflectance and transmittance spectra show clear resonance signatures for both A and B arrays (figures 3(b) and (c) for array A and figures 3(e) and (f) for array B). Besides a grating state sharp peak at the array periodicity (indicated as II in figure 3), we observed a blue-shifted peak (I) and a broad red-shifted resonance (III) for both A and B arrays [10]. As outlined in [14], periodic metallic gratings show a number of peculiar features in their spectra that depend mainly on the geometrical parameters of the structure. In particular, the dip shown as II corresponds to the excitation of a leaky mode that propagates on the metal grating and causes a sharp dip in the reflection spectrum while the other dip, indicated as III, is a hybrid state related to the availability of a Fabry-Pérot mode inside the cavity which propagates in the metal-insulator-metal (MIM) waveguide [14]. The presence of the MIM waveguide is responsible for the high transmission in figure 3. Interestingly, we found that the

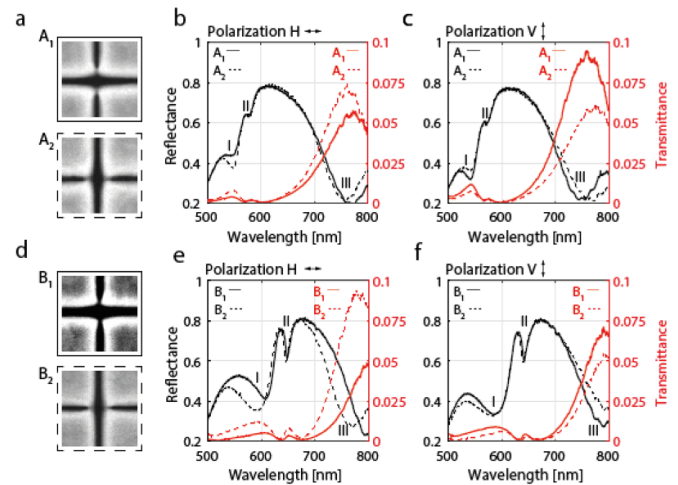


Figure 3. (a) Nano-gap orientation in array A₁ and array A₂, milled at period $P_A = 550$ nm with V-H and H-V order, respectively. (b) Reflectance (black) and transmittance (red) spectra for A₁ (solid line) and A₂ (dashed line) for H-polarized light. (c) As in (b) for V-polarized light. (d) Nano-gap orientation in array B₁ and array B₂, milled at period $P_B = 630$ nm with V-H and H-V groove order, respectively. (e) As in (b) for B₁ and B₂ arrays. (f) As in (c) for B₁ and B₂ arrays.

milling order influences the spectral response by shaping the NP morphology. For both A and B arrays, we measured a higher transmittance when the impinging light was polarized along the first-milled direction: V for A₁ and B₁ and H for A₂ and B₂ (figures 3(b) and (c) for array A and figures 3(e) and (f) for array B). We also observed that the transmittance is maximized ($\sim 10\%$) when the optimal illuminating polarization—V for A₁ and B₁, H for type A₂ and B₂—encountered narrow gaps in the perpendicular direction.

To describe the physical origin of the measured spectra we developed a theoretical model of the FIB-milled NP-arrays. We modelled the nano-platelets with a trapezoidal gold patches placed on top of the glass substrate, following figure 1(a).

The width w of the V grooves was set as 32 nm at the bottom (glass-gold interface) and 67 nm and 103 nm for vertical and horizontal milling, respectively. The gold thickness was set as 180 nm. This resulted in grooves with opening angles of $\alpha = 11.1^\circ$ for vertical milling and $\alpha = 22.3^\circ$ for horizontal milling. We did not take into account milling artifacts such as rounded corners.

The device optical response was studied by means of finite difference time domain (FDTD) and rigorous coupled-wave analysis (RCWA) methods (FullWave and DiffractMODE software from RSoft). We used a Drude-Lorentz model for gold consisting of a Drude pole and two Lorentz poles [17] for both numerical methods.

The relative complex permittivity is described in equation (1), where ϵ_∞ is metal dielectric constant at the high frequency regime in the Drude model, ω_D and γ_D are the plasma and collisions frequencies of free electron gas related to Drude model, whereas δ_i , ω_i and γ_i , $i = 1, 2$, are amplitude, resonant angular frequency and damping constant of

each Lorentz-like oscillator, respectively.

$$\varepsilon_m(\omega) = \varepsilon_\infty - \frac{\omega_D^2}{\omega^2 + j\omega\gamma_D} - \sum_{k=1}^2 \frac{\delta_k \omega_k^2}{\omega^2 - \omega_k^2 + 2j\omega\gamma_k} \quad (1)$$

A recent experimental study reported that the dielectric function of the metals is determined by their structural morphology and it strongly depends upon the film thickness [16]. We tuned a parameter γ_D ($1.66938 \times 10^{15} \text{ rad s}^{-1}$) called damping rate (or scattering loss) in order to analyze the influence of film thickness on the optical absorption and adjust the fitting parameters. First, we considered a periodic structure with array B1 parameters illuminated by a plane wave impinging at normal incidence. The structure had periodic boundary conditions along the x -axis and absorbing boundary conditions along the z -axis (figure 1(a)). Figure 4(a) shows the reflectance and the transmittance spectra of the periodic grating structure from FDTD simulations. A dip can be observed at a wavelength of 630 nm in the reflection spectrum. RCWA simulations for the infinite structure revealed that the spectra are based on contributions from all the grating orders ($0, \pm 1$).

However, the measured spectra (figure 3) showed another dip near 600 nm (shown as I in figure 3) which is not visible in the spectra shown in figure 4(a). We believe this first dip is due to missing diffraction orders ± 1 . This is because the experimental setup exploits a spot that illuminates a finite number of NPs (inset of figure 2). Hence, under normal incidence, the diffracted higher order modes could not be collected by the lens.

In order to match the experimental setup, the numerical model—based on real device dimensions—considered a limited number of grating periods and employed absorbing boundary conditions in all four directions in the XZ plane for FDTD simulations. The grating structure was illuminated by a normally incident Gaussian pulsed source with a Gaussian spatial profile (transverse magnetic (TM) polarization, electric field along the x -axis— E_x —as in figure 1(a)) centered at 600 nm. Figures 4(b) and (c) show the numerical reflectance and transmittance spectra when the Gaussian illumination diameter covers 20 NPs (beam waist equal to 10 periods). As it can be inferred from the plot, when considering a finite-size device, the shape and features of the simulated spectra match the experimental results and a dip (I) emerges at the blue side of the reflection spectra for both arrays A ($p = 550 \text{ nm}$) and B ($p = 630 \text{ nm}$). In particular for arrays B, FDTD simulations confirm that the first dip (I) is due to the first-order diffraction that is not collected in the experimental setup. Also, the simulated transmission agrees well with the experimental results, while previous work reported that ion beam bombardment increases the optical density of glass, reducing the transmission for wavelengths in the 500–600 nm range [18]. We suggest that the effect of ion beam bombardment is mitigated by the limited exposure of quartz during the milling process.

It can be furthered observed from figure 4(d) that under increasing width of the illuminating beam waist from 5 to 40 periods, dip I is red-shifting and decreasing in intensity eventually matching the results for an infinite structure. Conversely,

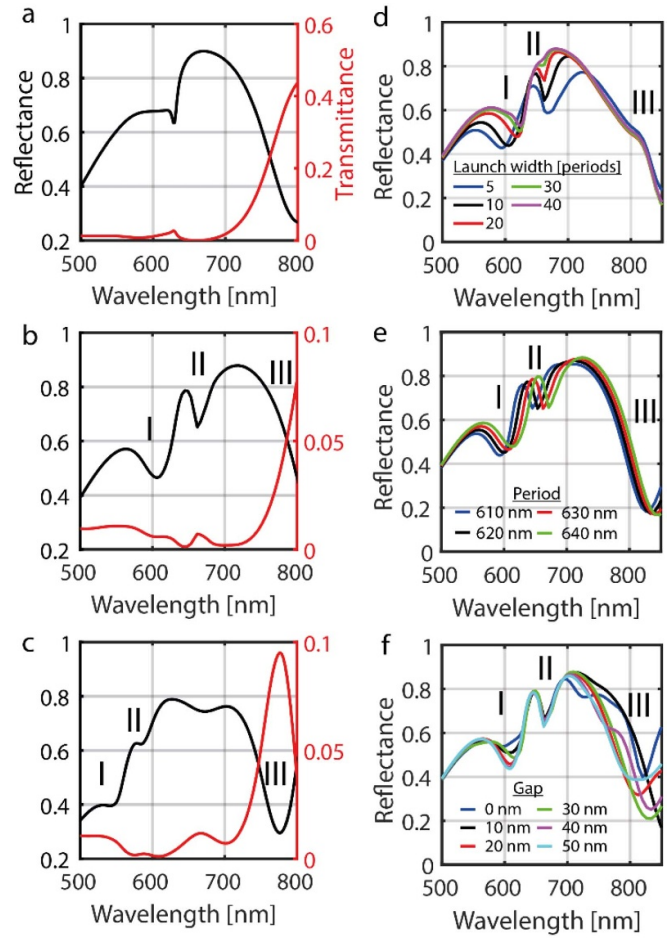


Figure 4. (a) Reflectance (black) and transmittance (red) spectra for infinite arrays of gold NPs, with periodicity $p = 630 \text{ nm}$ calculated with FDTD method. (b) FDTD simulation of reflectance (black) and transmittance (red) for a normally incident Gaussian beam pulse with a Gaussian spatial profile (TM polarization, centred at 600 nm) (c) As in (b) for $p = 550 \text{ nm}$. (d)–(f) Effect of the variation of the illumination beam waist (d), of the array periodicity (e) and of the bottom gap size w (f) on the reflectance spectrum.

the dip II is blue shifted and moves towards $\lambda = p$ as for the infinite structure (figure 4(b) and (c)).

To fully account for the effect of variations in the NP geometry, we modelled the reflectance and transmittance spectra while varying the array period and the gap size. As expected, a variation of the array periodicity shifts all the spectral features consistently (figure 4(e)). On the other hand, an increase on the gap width w (figure 1(a)) from 0 to 50 nm only alters the magnitude and position of the dips around 600 nm (I) and 800 nm (III) (figure 4(f)). This can explain the small difference in the position of the peaks in the range 750–800 nm in the experimental spectra. Overall, these numerical results confirmed our hypothesis, since simulations are in very good agreement with the measurements.

On the strength of the theoretical model developed, we predicted and validated the performances of the NPs array as a refractive index sensor. To do this, we first simulated the reflectivity spectrum for a NP array with $p = 630 \text{ nm}$ covered

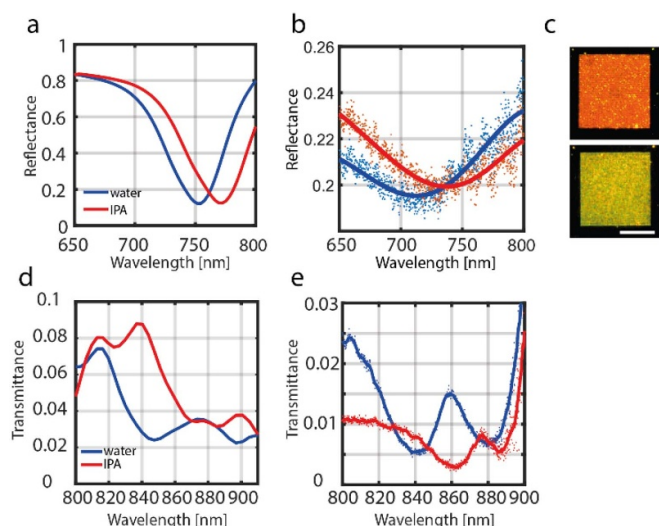


Figure 5. (a) Simulated spectral shift of the reflected light when a thin film of distilled water (blue line) or isopropyl alcohol (red line) covers the NP array with periodicity $p = 630$ nm. (b) Reflectance spectra measured with the array immersed in distilled water (blue dots) or IPA (red dots). Blue and red lines, serving as a guide to the eye, are obtained by interpolating the data with second-order Fourier series. (c) Dark field images of a NP array with periodicity $p = 550$ nm covered in air (top) or IPA (bottom). Scale bar is $15 \mu\text{m}$. (d) As in (a) for transmitted light for a NPs array with $p = 630$ nm. (e) Transmittance spectra measured with the array immersed in distilled water (blue dots) or IPA (red dots). Blue and red lines represent a moving average of the spectra over 3 nm.

in a thin layer of distilled water ($\text{RI} = 1.33$) and isopropyl alcohol (IPA) ($\text{RI} = 1.37$). Figure 5(a) shows that the numerical reflectance spectrum in IPA is red-shifted when compared to the reflection in water. The wavelength shifts (20 nm) results in a predicted sensitivity $S_R = 500 \text{ nm RIU}^{-1}$ and FOM, defined as $\text{FOM} = S/\Delta\lambda$ where $\Delta\lambda$ is the full width at half-maximum FWHM $= 50$ nm of the reflectance dip, of $\text{FOM} = 10 \text{ RIU}^{-1}$.

It is worth highlighting that numerical results show that similar performance, in terms of sensitivity and FOM, can be achieved by considering a lower number of the illuminated nanoplatelets ($N = 5$ or 10). However, for smaller launch widths, a flattened dip arises and this could increase the measurement uncertainty. We verified this prediction experimentally by acquiring the reflection spectra when the array ($p = 630$ nm) was covered by a thin layer of distilled water or IPA. The spectra in figure 5(b) show a clear red shift of the resonance when water is substituted with IPA ($\Delta\lambda = 24.9 \pm 5.3$ nm). As IPA was very volatile upon illumination of the array, the acquisition was limited to 3 s per analyte. The spectral shift was measured with the aid of visual eye-guides obtained by interpolating the data with second order Fourier series (figure 5(b)). When compared with the variation of refractive index unit (RIU), the wavelength shift translates to a sensitivity of $622 \pm 134 \text{ nm RIU}^{-1}$, compatible with the simulated value. The experimental figure of merit results as $\text{FOM} = 7 \text{ RIU}^{-1}$ for a FWHM $= 88$ nm.

To provide evidence of a fast, alternative detection method, we used dark field (DF) microscopy to image the array immersed in air or IPA. Using an upright microscope in DF configuration (Nikon Eclipse 2000), we illuminated the sample with oblique light: while the zeroth diffraction order was blocked, the first order reached the detector. We acquired DF images with the sample ($p = 550$ nm) covered in air and in IPA (figure 5(c)). It is apparent that only the patterned area produces a diffraction spectrum, as no signal arises from the gold layer around the platelets, apart from scattering from small particles deposited on the sample.

Similarly, we characterized the sensing performances using transmitted light. Figure 5(d) shows the numerical model for transmitted light when a $3 \mu\text{m}$ thick drop of water (blue) or IPA (red) covers the array ($p = 630$ nm). The change in refractive index induces a shift of the transmittance peak of $\Delta\lambda = 24$ nm; this shift implies that the array has a theoretical sensitivity of $S_T = 600 \text{ nm RIU}^{-1}$ and a $\text{FOM}_T = 24 \text{ RIU}^{-1}$ in transmission once the FWHM $= 25$ nm of the water peak is taken into account. The experimental measurements, shown in figure 5(e), produced a shift of $\Delta\lambda = 17.8 \pm 0.5$ nm that reflects a sensitivity of $S_T = 445 \pm 12 \text{ nm RIU}^{-1}$ and a $\text{FOM} = 29 \text{ RIU}^{-1}$, once the FWHM $= 15.4$ nm of the water peak is taken into account. While we attribute the differences between simulations and experiments to a mismatch in the thickness of simulated and actual layers of water and IPA, we observe that the measured values are consistent with literature reports on similar sensor architectures [8].

3. Conclusions

We have provided a comprehensive experimental and theoretical description of the combination of plasmonic and diffractive effects in finite, 2D arrays of NPs with sub-20 nm gaps fabricated with Ga FIB milling. Notably, we observed that high optical transmission (approaching 10%) can be achieved by illuminating a small number of elements (illumination beam diameter covers 20 periods). We have also proven that our arrays can serve as an effective refractive index sensors using either reflected or transmitted light. We envision that our work will favour future research on the fabrication of metallic nanostructures, on the fundamental investigation of their optical properties as well as on the application of these tools as advanced biosensors.

Acknowledgments

The authors thank C. Biagini and Dr. A. Toma of the IIT Clear Room facility.

Funding

FiP, AB, FeP acknowledge funding from the European Research Council under the European Union's Horizon 2020 research and innovation program (#677683). MP and MDV acknowledge funding from the European Research Council

under the European Union's Horizon 2020 research and innovation program (#692643). MP, LS, FeP and MDV are funded by the US National Institute of Health (1UF1NS108177-01). FeP and MDV acknowledge that project leading to this application has received funding from the European Union's Horizon 2020 research and innovation programme under grant agreement No 828972.

Conflict of interest

L.S., M.D.V. and F. Pisanello are founders and hold private equity in OptogeniX, a company that develops, produces and sells technologies to deliver light into the brain.

ORCID iDs

Filippo Pisano  <https://orcid.org/0000-0002-5499-160X>
 Antonio Balena  <https://orcid.org/0000-0003-4314-4314>
 Muhammad Fayyaz Kashif  <https://orcid.org/0000-0002-7837-6679>
 Marco Pisanello  <https://orcid.org/0000-0003-2179-7883>
 Gaia de Marzo  <https://orcid.org/0000-0002-8073-9395>
 Luciana Algieri  <https://orcid.org/0000-0003-3667-5432>
 Antonio Qualtieri  <https://orcid.org/0000-0002-2207-8111>
 Tiziana Stomeo  <https://orcid.org/0000-0001-5655-3104>
 Ferruccio Pisanello  <https://orcid.org/0000-0002-1489-7758>
 Marco Grande  <https://orcid.org/0000-0002-1906-8772>

References

- [1] Ebbesen T W, Lezec H J, Ghaemi H F, Thio T and Wolff P A 1998 Extraordinary optical transmission through sub-wavelength hole arrays *Nature* **391** 667–9
- [2] de Ceglia D, Vincenti M A, Scalora M, Akozbek N and Bloemer M J 2011 Plasmonic band edge effects on the transmission properties of metal gratings *AIP Adv.* **1** 032151
- [3] Porto J A, García-Vidal F J and Pendry J B 1999 Transmission resonances on metallic gratings with very narrow slits *Phys. Rev. Lett.* **83** 2845–8
- [4] Martín-Moreno L, García-Vidal F J, Lezec H J, Pellerin K M, Thio T, Pendry J B and Ebbesen T W 2001 Theory of extraordinary optical transmission through subwavelength hole arrays *Phys. Rev. Lett.* **86** 1114–7
- [5] Laluet J-Y, Devaux E, Genet C, Ebbesen T W, Weeber J-C and Dereux A 2007 Optimization of surface plasmons launching from subwavelength hole arrays: modelling and experiments *Opt. Express* **15** 3488
- [6] Tong L, Wei H, Zhang S and Xu H 2014 Recent advances in plasmonic sensors *Sensors (Basel)* **14** 7959–73
- [7] Mejía-Salazar J R and Oliveira O N 2018 Plasmonic biosensing *Chem. Rev.* **118** 10617–25
- [8] Xu Y, Bai P, Zhou X, Akimov Y, Png C E, Ang L-K, Knoll W and Wu L 2019 Optical refractive index sensors with plasmonic and photonic structures: promising and inconvenient truth *Adv. Opt. Mater.* **7** 1801433
- [9] Kostovski G, Stoddart P R and Mitchell A 2014 The optical fiber tip: an inherently light-coupled microscopic platform for micro- and nanotechnologies *Adv. Mater.* **26** 3798–820
- [10] Sloyan K, Melkonyan H and Dahlem M S 2020 Focused ion beam milling for prototyping 2D and 3D photonic structures *Int. J. Adv. Manuf. Technol.* **107** 1–12
- [11] Principe M, Consales M, Micco A, Crescitelli A, Castaldi G, Esposito E, La Ferrara V, Cutolo A, Galdi V and Cusano A 2017 Optical fiber meta-tips *Light Sci. Appl.* **6** e16226
- [12] Wang Q and Wang L 2020 Lab-on-fiber: plasmonic nano-arrays for sensing *Nanoscale* **12** 7485–99
- [13] La Ferrara V, Aneesh P M, Delli Veneri P, Mercaldo L V, Usatii I, Polichetti T, Ricciardi A, Quero G and Cusano A 2014 Focused ion beam strategy for nanostructure milling in doped silicon oxide layer for light trapping applications *Vacuum* **99** 135–42
- [14] Grande M et al 2011 Experimental demonstration of a novel bio-sensing platform via plasmonic band gap formation in gold nano-patch arrays *Opt. Express* **19** 21385
- [15] Søndergaard T, Bozhevolnyi S I, Novikov S M, Beermann J, Devaux E and Ebbesen T W 2010 Extraordinary optical transmission enhanced by nanofocusing *Nano Lett.* **10** 3123–8
- [16] Lin Y-Y, Liao J-D, Ju Y-H, Chang C-W and Shiau A-L 2011 Focused ion beam-fabricated Au micro/nanostructures used as a surface enhanced Raman scattering-active substrate for trace detection of molecules and influenza virus *Nanotechnology* **22** 185308
- [17] Yakubovsky D I, Arsenin A V, Stebunov Y V, Fedyanin D Y and Volkov V S 2017 Optical constants and structural properties of thin gold films *Opt. Express* **25** 25574
- [18] Fu Y and Bryan N K A 2005 Investigation of physical properties of quartz after focused ion beam bombardment *Appl. Phys. B* **80** 581–5